

Multi-Task Lung Nodule Detection in Chest Radiographs with a Dual Head Network

Chen-Han Tsai¹ and Yu-Shao Peng¹

HTC DeepQ
{maxwell_tsai,ys_peng}@htc.com

Abstract. Lung nodules can be an alarming precursor to potential lung cancer. Missed nodule detections during chest radiograph analysis remains a common challenge among thoracic radiologists. In this work, we present a multi-task lung nodule detection algorithm for chest radiograph analysis. Unlike past approaches, our algorithm predicts a global-level label indicating nodule presence along with local-level labels predicting nodule locations using a Dual Head Network (DHN). We demonstrate the favorable nodule detection performance that our multi-task formulation yields in comparison to conventional methods. In addition, we introduce a novel Dual Head Augmentation (DHA) strategy tailored for DHN, and we demonstrate its significance in further enhancing global and local nodule predictions.

Keywords: Nodule Detection · Chest Radiograph · Dual Head Network · Dual Head Augmentation · Faster R-CNN

1 Introduction

Lung cancer ranks among the top causes of cancer-related deaths worldwide. Pulmonary nodule findings, though typically benign, are an alarming sign for potential lung cancer. Given its simple and inexpensive operating cost, chest radiography (i.e., x-rays) is the most widely adopted chest imaging solution available. However, one concern during radiograph analysis is the proportion of nodules thoracic radiologists often miss due to the nature of the imaging modality [5, 26]. A chest radiograph is a 2D projection of a patients' chest. Thus, nodules appear less visible when occluded by other organs (e.g., rib cages) or foreign bodies (e.g., CVADs). With the rising workload already posing a challenge for thoracic radiologists, assistive tools to reduce missed nodules during chest radiograph analysis are gaining significant clinical relevance [4, 10, 19].

To identify pulmonary nodules on chest radiographs, several works propose potential solutions. Some [1, 21, 28] focus on image-level prediction indicating nodule presence per scan (we refer to as *global* methods). Others [11, 13, 18, 24] study patch-level prediction exploring nodule detection with local bounding box information for each nodule (we refer to as *local* methods). Although both local and global methods offer information regarding nodule presence in a given chest radiograph, adopting just a single method alone can be undesirable. Local

methods offer the benefit of pinpointing each nodule, but the adopted labeling criterion can be highly subjective and prone to inconsistency [2,12]. Global methods alleviate this issue by predicting a single label indicating nodule presence, but further effort is required by the examiner to locate these nodules.

Li et al. [14] and Pesce et al. [20] attempted to address this disparity. The former formulated a multiple instance learning (MIL) model to classify nodule presence using a grid of patches across the input scan. The image-level label is then computed using the joint probability across patch predictions. Despite its attempt in combining local and global predictions, such MIL model is not translation equivariant by design, causing the predicted global label to be highly dependent on the nodule location innate to the scan. The latter proposed CONAF, a network composed of a shared backbone between its classification and localization head. The classification head outputs a global label indicating nodule presence, and its localization head outputs a downsized score map. Considering that most nodule sizes are relatively small with respect to the scan size, the low resolution scoremap limits the localizer head from explicit localization purposes.

In this work, we present a novel multi-task lung nodule detection algorithm using a Dual Head Network (DHN) and an accompanying Dual Head Augmentation (DHA) training strategy. Our multi-task objective is similar to [3], but instead of using a RetinaNet [16], we adopt a modified Faster-RCNN [22] architecture customized for nodule detection. Considering the properties of pulmonary nodule, we propose to use deformable convolutions [6] and the gIOU loss [23]. In addition, we incorporate our novel DHA strategy during DHN training, and we demonstrate its importance in further enhancing global and local nodule predictions. The remaining of the paper is organized as follows. We first illustrate the preliminaries in Section 2. The proposed methods will be detailed in Section 3, followed by experimental results in Section 4. Conclusion will be given in Section 5.

2 Preliminaries

The Faster-RCNN [22] is a two-stage network originally designed for object detection. The first stage of the network is a feature extractor (i.e. VGG-16 [25]), and the second stage consists of an RPN, ROI Pool, and ROI Head module. For a given input image, the feature extractor outputs a feature representation of that image, and this representation is fed to the second stage. The RPN generates bounding box proposals around regions that contain potential non-background objects. Crops for each proposed region are then taken from the extracted feature representation, and they are resized to a fixed dimension using ROI Pool. The fixed-size feature crops are then independently classified using the ROI Head, and an updated bounding-box is predicted for each crop.

Modern implementations of the Faster-RCNN often include two modifications to the original design that enhances detection performance. The first is the attachment of the Feature Pyramid Network (FPN) [15] behind the first stage feature extractor. FPN allows cross-level information flow between multi-

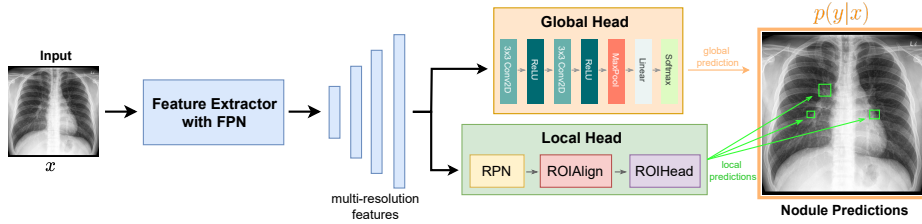


Fig. 1. An illustration of the DHN architecture during inference. The input x is fed through a feature extractor with FPN to obtain a set of multi-resolution features. The *global head* predicts the global label indicating nodule presence in the scan, and the *local head* predicts local bounding boxes indicating nodule locations.

resolution representations which is beneficial for detecting small objects. The second is the replacement of ROI Pool with Multi-Scale ROI Align [7, 15] to avoid quantization while cropping the multi-resolution features.

During training, the RPN generates an objectness loss ℓ_{obj} from the background foreground classification and a regression loss ℓ_{reg} from the distance computed between the proposed regions with their matched ground truth bounding boxes. The ROIHead generates a classification loss ℓ_{cls} during feature crop classification and a bounding box loss ℓ_{bbox} from the distance computed between the updated bounding boxes and their matched ground truth bounding boxes. The default setup utilizes a Smooth L1 Loss to train ℓ_{reg}, ℓ_{bbox} and the Cross Entropy Loss to train ℓ_{obj}, ℓ_{cls} . The final loss function L_{local} is formulated in Equation 1

$$L_{local} = \ell_{obj} + \ell_{reg} + \ell_{cls} + \ell_{bbox}. \quad (1)$$

3 Methods

In this section, we present our multi-task Dual Head Network (DHN) architecture and the accompanying Dual Head Augmentation (DHA) strategy. The DHN takes advantage of the two-stage structure seen in the Faster-RCNN by adding an additional network in parallel to the original second stage. The DHA strategy is applied during training, and it utilizes the DHN’s dual head design in improving nodule detection performance. The specifics are detailed in the following sections.

3.1 Dual Head Network

The DHN architecture is designed in a two-stage approach (see Figure 1). The first stage is a feature extractor with FPN, and the second stage consists of two parallel networks that we refer to as the *global head* and the *local head*. For a given scan, the feature extractor first extracts its respective representation. Then, the *global head* predicts a binary label indicating nodule presence, and the *local head* predicts bounding boxes around each detected nodule.

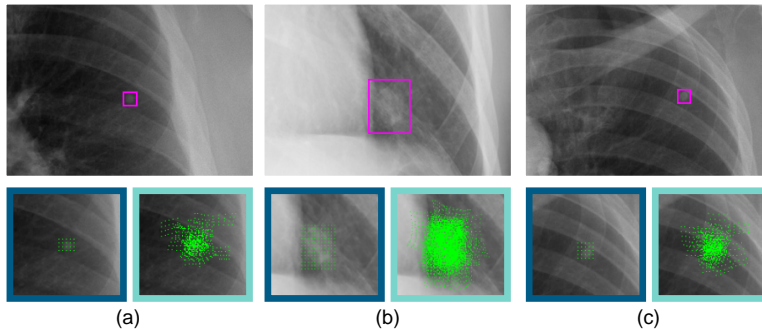


Fig. 2. Comparison between deformable (turquoise) versus standard convolution (dark blue) applied on three sample cases (a-c) using the 3rd layer of a trained ResNet-18 feature extractor. The receptive fields are fixed if regular convolution is applied, whereas deformable convolutions allow dynamic focus on the regions of interest.

The feature extractor of our DHN is a modified ResNet-18 [8]. We conduct a series of experiments comparing various CNN architectures from the ResNet family, and we observe slightly better performance as model size increased. However, the training time increases significantly for larger models. Hence, we select the smallest model from the ResNet family, the ResNet-18, to serve as a lower bound for DHN performance throughout our experiments. We modify the ResNet-18 by replacing standard convolutions with deformable convolutions [6] in the final three layers. Applying deformable convolutions allows more dynamic focus on particular regions in the image where the nodules size might be small (see Figure 2). For a given scan x , we take the intermediate representations the ResNet-18 extracts, and we pass them to the FPN to obtain set of multi-resolution representations. This set of multi-resolution representations is fed to the *global* and *local heads* for further processing.

The *global head*'s primary purpose is to classify whether nodules are present in a given scan. Thus, we select the representation with the largest receptive field [17] as input. As shown in Figure 3, this representation is passed through two consecutive 2D convolutions and ReLUs before being max-pooled into a single vector. Then, a linear layer and a softmax layer are applied to obtain the probability indicating nodule presence in the scan. For a set of N labeled scans $\{(x_i, y_i)\}_{i=1}^N$ where $x_i \in \mathbf{R}^{h \times w}$ is the i^{th} scan with resolution $h \times w$ (we set $h, w = 512$) and $y_i \in \{0, 1\}$ is the corresponding global label, we formulate the *global head loss* L_g (see Equation 2) using a weighted cross-entropy:

$$L_g = - \sum_i^N \alpha_1 y_i \log(p(y_i|x_i)) + \alpha_2 (1 - y_i) \log(1 - p(y_i|x_i)), \quad (2)$$

where α_1 and α_2 are two hyperparameters.

The *local head* serves as a nodule detector, and we adopt the second-stage design as specified in Section 2. During training, however, we replace the Smooth L1

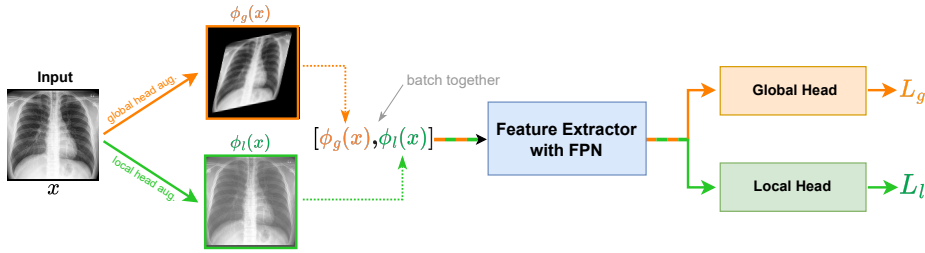


Fig. 3. An illustration of DHA. Two augmented images $\phi_g(x)$ and $\phi_l(x)$ of x are generated. They are batched together and passed into the feature extractor with FPN. The output features are then split according to their corresponding head. Individual head losses L_g and L_l are summed during training. Notice that $\phi_g(x)$ only updates the *global head*, and $\phi_l(x)$ only updates the *local head* during back-propagation.

loss in the RPN and the ROIHead with the gIOU loss [23] since the gIOU’s scale-invariant property is beneficial during small scale bounding box optimization. The *local head loss* L_l follows the formulation in Equation 1. We propose an end-to-end optimization method to consider the *local head loss* and the *global head loss* simultaneously. The final multi-task loss L (see Equation 3) is a weighted sum of the two losses, i.e.,

$$L = \lambda_1 L_g + \lambda_2 L_l. \quad (3)$$

3.2 Dual Head Augmentation

Data augmentation is a well-known technique that increases diversity in the training data to improve model generalization. In classical image classification or object detection tasks, one augmentation strategy (i.e., a pre-defined set of stochastic transforms) is applied per training image during the forward-pass. However, training with just one augmentation strategy per image for a dual head architecture can easily lead to one head being particularly optimized while the other head performs mediocly.

To fully optimize each head to their specific objectives, we propose a novel data augmentation strategy called the Dual Head Augmentation (DHA). DHA takes advantage of the DHN’s dual head structure by applying an augmentation strategy for each head. As shown in Figure 3, we designate an augmentation function ϕ_g for the *global head* and ϕ_l for the *local head*. Given an input scan x , the augmented images $\phi_g(x)$ and $\phi_l(x)$ are generated and batched together. This batch is fed into the feature extractor with FPN, and we obtain the multi-resolution representations. We split the batch, and we feed the representations corresponding to $\phi_g(x)$ and $\phi_l(x)$ to the *global* and *local heads* respectively to optimize each head.

We select a set of image transformations¹ that involves illumination transforms (e.g., histogram equalization, random brightness, etc.) and geometric trans-

¹ The complete list of transformations are detailed in the supplementary materials.

Model	Classification Metrics		Localization Metrics		
	ROC-AUC	PR-AUC	FROC-AUC	AFROC-AUC	mAP
FCOS [27]	-	-	0.540 ± 0.054	0.564 ± 0.024	0.166 ± 0.009
RetinaNet [16]	-	-	0.576 ± 0.009	0.507 ± 0.023	0.166 ± 0.003
DenseNet-121 [9]	0.856 ± 0.006	0.612 ± 0.006	-	-	-
CONAF [20]	0.800 ± 0.004	0.450 ± 0.007	-	-	-
Global Head only	0.809 ± 0.010	0.524 ± 0.014	-	-	-
Local Head only	-	-	0.618 ± 0.006	0.606 ± 0.029	0.184 ± 0.008
DHN	0.873 ± 0.004	0.654 ± 0.016	0.628 ± 0.011	0.626 ± 0.033	0.188 ± 0.009

Table 1. Performance comparison between the DHN and alternate methods trained without data augmentation.

forms (e.g., horizontal flip, rotation, etc.). In this work, we consider two types of augmentation strategies that exhibit favorable single-head performance, and we define the augmentation strategies by their sampling method. The first sampling method is binomial sampling. Formally, for a given probability p and a set of transforms $\Theta = \{\theta_j\}_{j=1}^M$, binomial sampling selects transform θ_j for $j \in \{1, \dots, M\}$ with probability p , and we refer to the corresponding augmentation strategy as $\phi^{\text{bin}}(x; p, \Theta)$. The second sampling method is uniform sampling. Specifically, uniform sampling selects a transform from Θ with probability $1/M$, and we refer to this augmentation strategy as $\phi^{\text{uni}}(x; \Theta)$. During each training iteration, the augmentation strategy samples from Θ using one of the above sampling methods and applies the selected transforms.

4 Experiments

In this section, we evaluate the nodule detection performance of a DHN in comparison to other notable approaches. In addition, we perform a series of experiments to compare the influence different augmentation strategies play towards enhancing global and local predictions. Classification performance is evaluated using the *global head* prediction, and localization performance² is evaluated with *local head* predictions. We report on the test set mean and standard deviation of the top 8 performing validation checkpoints throughout each experiment. Each model is trained with SGD and momentum for 70 epochs (~ 3 days on an NVIDIA P100 16GB GPU) with a step size of $5e-5$ and momentum of 0.975 at a batch size of 2. Loss weights α_1, α_2 are set to 0.69 and 1.76 while λ_1, λ_2 are set to 0.35 and 2.5.

4.1 Dataset

The dataset we evaluate in this study is a subset of the National Institute of Health (NIH) Chest X-Ray dataset [28]. Each case in our dataset was labeled

² FROC and AFROC are computed with an Intersection over Union (IOU) threshold of 0.4, and the FROC-AUC is computed with a False Positive Per-Image up to 1.

with bounding box annotations for each nodule by three thoracic radiologists. Prior to labeling, each radiologist had to pass an assessment test requiring them to correctly identify over 80% of the cases from a held-out test set with potential lung nodules. The radiologists were then asked to independently label each case in our dataset. Labels were aggregated upon completion, and the radiologists reviewed each case to reach a consensus on which labels to keep. A final senior radiologist then reviewed and control the quality of annotations. In total, we randomly sample 26000 scans from NIH dataset and 21,189 qualified scans are added to our dataset. These scans are split into training, validation, and test sets following the ratio of 80 : 10 : 10 based on patient identifiers.

4.2 Dual Head Network Analysis

For our first set of experiments, we evaluate the performance of a DHN in comparison to several *global* and *local* methods [9, 16, 27]. We also compare our DHN with a notable dual-head approach CONAF [20]. Although CONAF’s localization head generates a heatmap-like mask for nodule localization, the mask is too coarse to derive precise bounding box coordinates from. Hence, we only evaluate the classifier head’s prediction in our comparison. For fair comparison, we do not apply data augmentation to the training strategy. We also analyze the single head performance of the DHN. Specifically, we consider the case where we train only the *global head* and the case where we train only the *local head*.

As shown in Table 1, the DHN architecture yields favorable improvements in both classification and localization metrics. We believe this improvement is that our DHN extracts more informative representations due to cross-task supervision. Specifically, training with local labels using the *local head* encourages the feature extractor to extract more meaningful representations that highlight local findings. Since these representations are shared with the *global head*, classification can benefit from the available local information the representations possess. Conversely, global labels are trained with high level features that have the widest receptive field. This encourages the feature extractor to leverage potential ancillary information beneficial for global prediction which may also assist local predictions. As our experiments demonstrate, we observe complementing nodule detection performance from the two heads when they are jointly trained.

4.3 Dual Head Augmentation Evaluation

In this subsection, we are interested in analyzing the effects different augmentation strategies impose on the DHN’s global and local predictions. As mentioned in Section 3.2, we consider both binomial and uniform augmentation strategies ϕ^{bin} and ϕ^{uni} . We also include an identity transform (no augmentation) strategy denoted ϕ^{id} as a baseline reference.

We first analyze the performance of a DHN when only one augmentation strategy is applied on one of the two heads. From the results shown in Table 2, we can see that better classification performance is observed when the *global head* uses the strategy ϕ^{bin} . Similarly, we observe slightly better localization

DHA		Classification Metrics		Localization Metrics		
Global	Local	ROC-AUC	PR-AUC	FROC-AUC	AFROC-AUC	mAP
ϕ^{id}	ϕ^{id}	0.873 ± 0.004	0.654 ± 0.016	0.628 ± 0.011	0.626 ± 0.033	0.188 ± 0.009
ϕ^{bin}	ϕ^{id}	0.879 ± 0.007	0.675 ± 0.017	0.624 ± 0.012	0.575 ± 0.037	0.184 ± 0.006
ϕ^{uni}	ϕ^{id}	0.877 ± 0.004	0.673 ± 0.012	0.627 ± 0.009	0.597 ± 0.057	0.182 ± 0.06
ϕ^{id}	ϕ^{bin}	0.858 ± 0.007	0.631 ± 0.011	0.656 ± 0.009	0.687 ± 0.014	0.182 ± 0.007
ϕ^{id}	ϕ^{uni}	0.877 ± 0.003	0.643 ± 0.009	0.658 ± 0.017	0.663 ± 0.015	0.200 ± 0.005
ϕ^{bin}	-	0.849 ± 0.004	0.628 ± 0.007	-	-	-
ϕ^{uni}	-	0.834 ± 0.008	0.585 ± 0.019	-	-	-
-	ϕ^{bin}	-	-	0.637 ± 0.032	0.686 ± 0.028	0.177 ± 0.024
-	ϕ^{uni}	-	-	0.651 ± 0.021	0.662 ± 0.015	0.204 ± 0.008

Table 2. Comparison of single head DHA strategies (ϕ^{id} on one of the heads). First five rows are the results of joint training with single head DHA. The bottom four rows are the results when only a single head is trained with the specified augmentation strategy.

performance when the *local head* adopts the strategy ϕ^{uni} . We can also observe noticeable improvements with dual head training versus single head training. When only one augmentation strategy is employed on a single DHN head, its performance still surpasses that of a single head network that utilizes the same augmentation strategy. This observation reflects the results we perceive in Section 4.2. Thus, even when just one augmentation strategy is applied on a single DHN head, we can expect favorable performance from DHN’s over single head networks.

DHA		Classification Metrics		Localization Metrics		
Global	Local	ROC-AUC	PR-AUC	FROC-AUC	AFROC-AUC	mAP
ϕ^{bin}	ϕ^{bin}	0.882 ± 0.003	0.674 ± 0.008	0.668 ± 0.008	0.707 ± 0.013	0.187 ± 0.006
ϕ^{uni}	ϕ^{uni}	0.881 ± 0.009	0.675 ± 0.015	0.664 ± 0.008	0.702 ± 0.009	0.159 ± 0.012
ϕ^{bin}	ϕ^{uni}	0.903 ± 0.003	0.702 ± 0.003	0.708 ± 0.005	0.705 ± 0.008	0.245 ± 0.005
ϕ^{uni}	ϕ^{bin}	0.878 ± 0.003	0.667 ± 0.010	0.658 ± 0.011	0.676 ± 0.011	0.202 ± 0.005

Table 3. Comparison of dual head DHA strategies (i.e., ϕ^{bin} and ϕ^{uni} applied on the global and local heads).

With the observed characteristics for the *global* and *local head*, we propose a hypothesis that heavier augmentations ϕ^{bin} are more suitable for the *global head* but not necessarily the *local head*. We believe that the *global head* favors heavier augmentations to increase its robustness against image-level distortions. In contrary, the *local head* seems to prefer lighter augmentations as heavy augmentations might have imposed an overwhelming amount of distortions to region specific features. We verify our hypothesis with an experiment shown in Table 3. The results verify our hypothesis that the DHN obtains optimal performance when the DHA strategy applies ϕ^{bin} on the *global head* and ϕ^{uni} on the *local head*.

5 Conclusion

In this work, we present a multi-task lung nodule detection algorithm using a DHN. Our DHN architecture features a *global head* and a *local head* that performs lung nodule detection on the global and local level simultaneously. In addition, we introduce a novel DHA strategy that leverages the dual head design of the DHN to enhance global and local nodule detection performance while training. Throughout our experiments, we demonstrate the performance gain our DHN yields in comparison to conventional single head networks in both classification and localization abilities. Furthermore, we identified the DHA strategy that applies the appropriate augmentations for each head. Together with the optimal DHA strategy, our DHN obtained a performance otherwise not attainable if regular single head augmentation strategies are employed.

Acknowledgements We would like to thank Che-Han Chang and the anonymous reviewers for their valuable suggestions. We also thank the members: Chun-Nan Chou, Fu-Chieh Chang, Yu-Quan Zhang, and Hao-Jen Wang for their support in collecting annotated data, and Yi-Hsiang Chin for his efforts in conducting experiments.

References

1. Ausawalaithong, W., Thirach, A., Marukatat, S., Wilaiprasitporn, T.: Automatic lung cancer prediction from chest x-ray images using the deep learning approach. BMEiCON 2018 - 11th Biomedical Engineering International Conference (1 2019). <https://doi.org/10.1109/BMEiCON.2018.8609997>
2. Busby, L.P., Courtier, J.L., Glastonbury, C.M.: Bias in radiology: The how and why of misses and misinterpretations. *Radiographics* **38**, 236–247 (1 2018), <https://pubs.rsna.org/doi/abs/10.1148/rg.2018170107>
3. de Cea, M.V.S., Diedrich, K., Bakalo, R., Ness, L., Richmond, D.: Multi-task learning for detection and classification of cancer in screening mammography. *Lecture Notes in Computer Science (including subseries Lecture Notes in Artificial Intelligence and Lecture Notes in Bioinformatics)* **12266 LNCS**, 241–250 (10 2020). https://doi.org/10.1007/978-3-030-59725-2_24
4. Cha, M.J., Chung, M.J., Lee, J.H., Lee, K.S.: Performance of deep learning model in detecting operable lung cancer with chest radiographs. *Journal of thoracic imaging* **34**, 86–91 (3 2019). <https://doi.org/10.1097/RTI.0000000000000388>
5. del Ciello, A., Franchi, P., Contegiacomo, A., Cicchetti, G., Bonomo, L., Larici, A.R.: Missed lung cancer: when, where, and why? *Diagnostic and Interventional Radiology* **23**, 118 (3 2017). <https://doi.org/10.5152/DIR.2016.16187>
6. Dai, J., Qi, H., Xiong, Y., Li, Y., Zhang, G., Hu, H., Wei, Y.: Deformable convolutional networks. In: 2017 IEEE International Conference on Computer Vision (ICCV). pp. 764–773 (2017). <https://doi.org/10.1109/ICCV.2017.89>
7. He, K., Gkioxari, G., Dollár, P., Girshick, R.B.: Mask r-cnn. 2017 IEEE International Conference on Computer Vision (ICCV) pp. 2980–2988 (2017)
8. He, K., Zhang, X., Ren, S., Sun, J.: Deep residual learning for image recognition. 2016 IEEE Conference on Computer Vision and Pattern Recognition (CVPR) pp. 770–778 (2016)

9. Huang, G., Liu, Z., Maaten, L.V.D., Weinberger, K.Q.: Densely connected convolutional networks. Proceedings - 30th IEEE Conference on Computer Vision and Pattern Recognition, CVPR 2017 **2017-January**, 2261–2269 (11 2017). <https://doi.org/10.1109/CVPR.2017.243>
10. Hwang, E.J., Park, C.M.: Clinical implementation of deep learning in thoracic radiology: Potential applications and challenges. Korean Journal of Radiology **21**, 511–525 (5 2020). <https://doi.org/10.3348/KJR.2019.0821>
11. Kim, Y.G., Cho, Y., Wu, C.J., Park, S., Jung, K.H., Seo, J.B., Lee, H.J., Hwang, H.J., Lee, S.M., Kim, N.: Short-term reproducibility of pulmonary nodule and mass detection in chest radiographs: Comparison among radiologists and four different computer-aided detections with convolutional neural net. Scientific Reports 2019 9:1 **9**, 1–9 (12 2019). <https://doi.org/10.1038/s41598-019-55373-7>
12. Larici, A.R., Farchione, A., Franchi, P., Ciliberto, M., Cicchetti, G., Calandriello, L., del Ciello, A., Bonomo, L.: Lung nodules: size still matters. European respiratory review : an official journal of the European Respiratory Society **26** (12 2017). <https://doi.org/10.1183/16000617.0025-2017>
13. Li, X., Shen, L., Luo, S.: A solitary feature-based lung nodule detection approach for chest x-ray radiographs. IEEE Journal of Biomedical and Health Informatics **22**, 516–524 (3 2018). <https://doi.org/10.1109/JBHI.2017.2661805>
14. Li, Z., Wang, C., Han, M., Xue, Y., Wei, W., Li, L.J., Fei-Fei, L.: Thoracic disease identification and localization with limited supervision. In: 2018 IEEE/CVF Conference on Computer Vision and Pattern Recognition. pp. 8290–8299 (2018). <https://doi.org/10.1109/CVPR.2018.00865>
15. Lin, T.Y., Dollár, P., Girshick, R., He, K., Hariharan, B., Belongie, S.: Feature pyramid networks for object detection. In: 2017 IEEE Conference on Computer Vision and Pattern Recognition (CVPR). pp. 936–944 (2017). <https://doi.org/10.1109/CVPR.2017.106>
16. Lin, T.Y., Goyal, P., Girshick, R., He, K., Dollár, P.: Focal loss for dense object detection. In: 2017 IEEE International Conference on Computer Vision (ICCV). pp. 2999–3007 (2017). <https://doi.org/10.1109/ICCV.2017.324>
17. Luo, W., Li, Y., Urtasun, R., Zemel, R.: Understanding the effective receptive field in deep convolutional neural networks. In: Proceedings of the 30th International Conference on Neural Information Processing Systems. p. 4905–4913. NIPS’16, Curran Associates Inc. (2016)
18. Mendoza, J., Pedrini, H.: Detection and classification of lung nodules in chest x-ray images using deep convolutional neural networks. Computational Intelligence **36**, 370–401 (5 2020). <https://doi.org/10.1111/COIN.12241>
19. Nam, J.G., Park, S., Hwang, E.J., Lee, J.H., Jin, K.N., Lim, K.Y., Vu, T.H., Sohn, J.H., Hwang, S., Goo, J.M., Park, C.M.: Development and validation of deep learning-based automatic detection algorithm for malignant pulmonary nodules on chest radiographs. Radiology **290**, 218–228 (1 2019), <https://pubs.rsna.org/doi/abs/10.1148/radiol.2018180237>
20. Pesce, E., Withey, S.J., Ypsilantis, P.P., Bakewell, R., Goh, V., Montana, G.: Learning to detect chest radiographs containing pulmonary lesions using visual attention networks. Medical image analysis **53**, 26–38 (4 2019). <https://doi.org/10.1016/J.MEDIA.2018.12.007>
21. Rajpurkar, P., Irvin, J.A., Zhu, K., Yang, B., Mehta, H., Duan, T., Ding, D.Y., Bagul, A., Langlotz, C., Shpanskaya, K.S., Lungren, M.P., Ng, A.: Chexnet: Radiologist-level pneumonia detection on chest x-rays with deep learning. ArXiv [abs/1711.05225](https://arxiv.org/abs/1711.05225) (2017)

22. Ren, S., He, K., Girshick, R., Sun, J.: Faster r-cnn: Towards real-time object detection with region proposal networks. *IEEE Transactions on Pattern Analysis and Machine Intelligence* **39**(6), 1137–1149 (2017). <https://doi.org/10.1109/TPAMI.2016.2577031>
23. Rezatofghi, H., Tsoi, N., Gwak, J., Sadeghian, A., Reid, I., Savarese, S.: Generalized intersection over union: A metric and a loss for bounding box regression. In: 2019 IEEE/CVF Conference on Computer Vision and Pattern Recognition (CVPR). pp. 658–666 (2019). <https://doi.org/10.1109/CVPR.2019.00075>
24. Schultheiss, M., Schober, S.A., Lodde, M., Bodden, J., Aichele, J., Müller-Leisse, C., Renger, B., Pfeiffer, F., Pfeiffer, D.: A robust convolutional neural network for lung nodule detection in the presence of foreign bodies. *Scientific Reports* 2020 10:1 **10**, 1–9 (7 2020). <https://doi.org/10.1038/s41598-020-69789-z>
25. Simonyan, K., Zisserman, A.: Very deep convolutional networks for large-scale image recognition. In: *International Conference on Learning Representations* (2015)
26. Tack, D., Howarth, N.: Missed Lung Lesions: Side-by-Side Comparison of Chest Radiography with MDCT, pp. 17–26. Springer International Publishing, Cham (2019). https://doi.org/10.1007/978-3-030-11149-6_2
27. Tian, Z., Shen, C., Chen, H., He, T.: Fcos: Fully convolutional one-stage object detection. In: 2019 IEEE/CVF International Conference on Computer Vision (ICCV). pp. 9626–9635 (2019). <https://doi.org/10.1109/ICCV.2019.00972>
28. Wang, X., Peng, Y., Lu, L., Lu, Z., Bagheri, M., Summers, R.M.: Chestx-ray8: Hospital-scale chest x-ray database and benchmarks on weakly-supervised classification and localization of common thorax diseases. *2017 IEEE Conference on Computer Vision and Pattern Recognition (CVPR) 2017-January*, 3462–3471 (7 2017). <https://doi.org/10.1109/CVPR.2017.369>